symmetry

MDPI

*Article*

# Correlation of Neutrinoless Double-$\beta$ Decay Nuclear Matrix Element with $E2$ Strength

**Changfeng Jiao [1,*], Cenxi Yuan [2] and Jiangming Yao [1]**

[1] School of Physics and Astronomy, Sun Yat-sen University, Zhuhai 519082, China
[2] Sino-French Institute of Nuclear Engineering and Technology, Sun Yat-sen University, Zhuhai 519082, China
* Correspondence: jiaochf@mail.sysu.edu.cn

**Abstract:** We explore the correlation of the neutrinoless double-$\beta$ decay nuclear matrix element (NME) with electric quadrupole ($E2$) strength in the framework of the Hamiltonian-based generator-coordinate method, which is a configuration-mixing calculation of symmetry-restored intrinsic basis states. The restoration of symmetries that are simultaneously broken in the mean-field states allows us to compute the structural and decay properties associated with wave functions characterized by good quantum numbers. Our calculations show a clear anti-correlation between the neutrinoless double-$\beta$ decay NME and the transition rate of the collective quadrupole excitation from the ground state in response to artificial changes of the quadrupole–quadrupole interaction. The anti-correlation is more remarkable in the decay from a weakly deformed parent nucleus to a more deformed grand-daughter nucleus. This interrelation may provide a way to reduce the uncertainty of the nuclear matrix element.

**Keywords:** neutrinoless double-$\beta$ decay; generator-coordinate method; reduced $E2$ transition probability



**Citation:** Jiao, C.; Yuan, C.; Yao, J. Correlation of Neutrinoless Double-$\beta$ Decay Nuclear Matrix Element with $E2$ Strength. *Symmetry* **2023**, *15*, 552. https://doi.org/10.3390/sym15020552

Academic Editors: Feng Pan, Jerry Paul Draayer and Andriana Martinou

Received: 20 January 2023
Revised: 13 February 2023
Accepted: 16 February 2023
Published: 19 February 2023



## 1. Introduction

Large-scale experiments in search of neutrinoless double-beta ($0\nu\beta\beta$) decays are likely to determine whether neutrinos are Majorana fermions, and hence reveal corresponding new physics beyond the Standard Model of electroweak interactions. However, the estimation of the rate of $0\nu\beta\beta$ decay, which is crucial for a definitive choice and quantity of candidate nuclei required in these sophisticated experiments, depends on reliable descriptions of nuclear matrix elements (NMEs) [1]. In addition, if this extremely rare decay is observed, the measured decay rates can provide essential information for determining the absolute neutrino mass scale and mass hierarchy, but it relies on whether one can obtain an accurate description of the corresponding NMEs [1].

There are several nuclear structure methods for calculations of the $0\nu\beta\beta$ decay matrix elements. The most used ones are the shell model (SM) [2–10], the interacting boson model (IBM) [11–13], the quasiparticle random phase approximation (QRPA) [14–25], the generator coordinate method (GCM) based on energy density functional (EDF) [26–30] or effective Hamiltonian [31–34], the in-medium generator coordinate method (IM-GCM) [35], and the coupled-cluster (CC) method [36]. At present, NMEs predicted by these nuclear models differ by factors of 3 to 4 for most candidate nuclides, and up to 8 in the case of decay from $^{48}$Ca to $^{48}$Ti [37–39]. These large uncertainties preclude an efficient plan for experiments [37]. Reducing the uncertainty in the matrix elements thus becomes an urgent need in the nuclear structure community.

One way to improve the accuracy of $0\nu\beta\beta$ NME calculations is searching for their correlations with certain nuclear structure observables. Since the observables can be determined experimentally, it could help to pin down the values of $0\nu\beta\beta$ NMEs if there are strong correlations between them. It is found that some certain collective correlations influence significantly on the calculated $0\nu\beta\beta$ NMEs. In particular, the matrix elements

would be suppressed when the ground states of the grandparent and grand-daughter nuclei have different intrinsic deformations [40]. This suppression was originally investigated with axial quadrupole collectivity [26,28,29,41], and later extended to non-axial quadrupole [32] and octupole correlations [30]. This leads to an interesting question: whether there is a correlation between $0\nu\beta\beta$ NME and the observable in associate with quadrupole collectivity, e.g., the reduced $E2$ transition probability $B(E2)$.

Another interesting feature, which implies a potential correlation between $0\nu\beta\beta$ NME and $E2$ strength, is the Gamow-Teller (GT) transition strength. On one hand, since the GT transition replaces a neutron with a proton or the other way around, its strength of the grandparent to intermediate nuclei, combined with the strength of the grand-daughter to intermediate nuclei, is particularly related to double-$\beta$ decay. On the other hand, recent work has demonstrated a remarkable anti-correlation between the calculated Gamow-Teller strength and the reduced transition probability of the lowest collective $E2$ excitation [42]. Though the connection between the GT strength and $0\nu\beta\beta$ NME is not straightforward, it is quite natural to expect a similar correlation of $0\nu\beta\beta$ decay NME with the transition rate of the low-lying collective $E2$ excitation.

Therefore it would be of particular interest to modify the quadrupole–quadrupole term in the effective Hamiltonian and to examine how the $0\nu\beta\beta$ NME changes are correlated with the resultant $E2$ strength. It is worth noting that a statistical analysis for the $0\nu\beta\beta$ NME of $^{48}$Ca has been proposed recently by adding random contributions to three sets of $pf$-shell effective Hamiltonians, i.e., the FPD6, GXPF1A, and KB3G interactions [43]. It gives some hints that the $B(E2)$ values in $^{48}$Ti are correlated with the neutron occupation probabilities, and hence, indirectly influence the $^{48}$Ca-Ti $0\nu\beta\beta$ NME. It is natural to presume that, instead of random contributions, a detailed analysis of NME by adding a specific term directly related to quadrupole collectivity would be of great importance.

In this work, we propose an analysis of the $0\nu\beta\beta$ NMEs and their correlations with the reduced collective quadrupole transition probabilities $B(E2; 0^+ \rightarrow 2^+)$. It is obtained by adding a different amount of quadrupole–quadrupole contributions to the corresponding effective Hamiltonians, and then perform the Hamiltonian-based GCM [32,33] calculation using the modified effective Hamiltonians. We apply our analysis to $^{48}$Ca$-$Ti, $^{76}$Ge$-$Se, $^{124}$Sn$-$Te, $^{130}$Te$-$Xe, and $^{136}$Xe$-$Ba, which covers light-, medium-, and heavy-mass candidate nuclei associated with the $0\nu\beta\beta$ decay. We consider only the standard light left-handed Majorana neutrino exchange mass mechanism in this work, since it is the simplest and most studied mechanism of the $0\nu\beta\beta$ decay process.

## 2. The Model

Owing to the closure approximation, we can express the $0\nu\beta\beta$ decay matrix element in terms of a two-body $0\nu\beta\beta$ transition operator between the ground-state wave functions of the grandparent and grand-daughter nuclei. If the decay is originated from the exchange of light Majorana neutrinos with usual left-handed weak interaction, the NME can be obtained by:

$$M^{0\nu} = M^{0\nu}_{\mathrm{GT}} - \frac{g_V^2}{g_A^2} M^{0\nu}_{\mathrm{F}} + M^{0\nu}_{\mathrm{T}} \tag{1}$$

where GT, F, and T refer to the Gamow-Teller, Fermi and tensor parts of the matrix elements. $g_V$ and $g_A$ are the vector and axial coupling constants, which are taken as $g_V = 1$ and $g_A = 1.254$, respectively. Our wave functions are modified at short distances by using a Jastrow-type short-range correlation (SRC) function in the parametrization of CD-Bonn [19]. A more detailed expression of the matrix element can be found in Ref. [18].

To calculate the $0\nu\beta\beta$ matrix element in Equation (1), a key feature is the description of ground-state wave function of grandparent and grand-daughter nuclei, i.e., $|I\rangle$ and $|F\rangle$, which can be given by our GCM calculations. Firstly, we employ a shell-model effective

Hamiltonian ($H_{\text{eff}}$). In an isospin scheme, $H_{\text{eff}}$ can be written in terms of one- and two-body operators as the following:

$$H_{\text{eff}} = \sum_a \epsilon_a \hat{n}_a + \sum_{a \leqslant b, c \leqslant d} \sum_{JT} V_{JT}(ab;cd) \hat{T}_{JT}(ab;cd), \tag{2}$$

where $\epsilon_a$ and $V_{JT}(ab;cd)$ stand for the one-body and two-body matrix elements of the nucleon–nucleon interaction, respectively. $\hat{n}_a$ denotes the number operator for the spherical single-particle orbit $a$ labelled with quantum numbers $(n_a, l_a, j_a)$, and

$$\hat{T}_{JT}(ab;cd) = \sum_{MT_z} A^{\dagger}_{JMTT_z}(ab) A_{JMTT_z}(cd) \tag{3}$$

is the scalar two-body density operator for nucleon pairs occupied the spherical orbitals $a, b$ and $c, d$, which are coupled to the quantum numbers $J, M, T$, and $T_z$.

Changing adequately the effective Hamiltonian used in the calculations, one can increase or decrease the quadrupole correlations in grand-parent, grand-daughter, or both nuclei. In this manner, we can gauge the correlation of the decays with the $E2$ transition probabilities. We have artificially changed the quadrupole strength adding an extra quadrupole–quadrupole term, namely $\lambda \hat{Q} \cdot \hat{Q}$, to the effective interaction. Increasing the values of coupling constant $\lambda$ would increase the deformation and hence would enhance the $E2$ transition strength.

The next step in our GCM calculation is generating a reference state set $|\Phi(q)\rangle$. It consists of quasiparticle vacua constrained to different expectation values $q_i = \langle \mathcal{O}_i \rangle$ for a set of collective operators $\mathcal{O}_i$. In this work, we take the following operators $\mathcal{O}_i$:

$$\begin{aligned} \mathcal{O}_1 &= Q_{20}, & \mathcal{O}_2 &= Q_{22}, \\ \mathcal{O}_3 &= \frac{1}{2}(P_0 + P_0^{\dagger}), & \mathcal{O}_4 &= \frac{1}{2}(S_0 + S_0^{\dagger}), \end{aligned} \tag{4}$$

where

$$\begin{aligned} Q_{2M} &= \sum_a r_a^2 Y_a^{2M}, \\ P_0^{\dagger} &= \frac{1}{\sqrt{2}} \sum_l \hat{l} [c_l^{\dagger} c_l^{\dagger}]_{000}^{L=0,J=1,T=0}, \\ S_0^{\dagger} &= \frac{1}{\sqrt{2}} \sum_l \hat{l} [c_l^{\dagger} c_l^{\dagger}]_{000}^{L=0,J=0,T=1}, \end{aligned} \tag{5}$$

with $M$ standing for the projection of angular momentum on the $z$-axis, $a$ as a label of nucleons, and the brackets indicating the coupling of orbital angular momentum, spin, and isospin to different values, each of which has zero $z$-projection. The operator $c_l^{\dagger}$ in Equation (5) creates a particle occupying the single-particle orbital with an orbital angular momentum $l$, and $\hat{l} \equiv \sqrt{2l+1}$. In addition, the operator $P_0^{\dagger}$ ($S_0^{\dagger}$) creates a correlated isoscalar (isovector) proton–neutron pair in the single-particle level $l$. To include the proton–neutron pairing effect, we start from a Bogoliubov transformation that mixes protons and neutrons in the quasiparticle creation and annihilation operators, i.e., (schematically),

$$\alpha^{\dagger} \sim u_p c_p^{\dagger} + v_p c_p + u_n c_n^{\dagger} + v_n c_n. \tag{6}$$

In the practical calculations, the full equations should sum over single-particle states in the valence space, and hence we replace each of the coefficients $u'$s and $v'$s in Equation (6) with matrices $U$ and $V$, which can be found in Ref. [44].

We then solve the constrained Hartree-Fock-Bogoliubov (HFB) equations for the effective Hamiltonian with linear constraints:

$$\begin{aligned}\langle H' \rangle = \langle H_{\text{eff}} \rangle - \lambda_N(\langle N_N \rangle - N) - \lambda_Z(\langle N_Z \rangle - Z) \\ - \sum_i \lambda_i(\langle \mathcal{O}_i \rangle - q_i),\end{aligned} \tag{7}$$

where the $N_N$ and $N_Z$ signify the neutron and proton number operators, while $\lambda_N$ and $\lambda_Z$ stand for corresponding Lagrange multipliers. The sum over $i$ includes the quadrupole operators $Q_{20}$ and $Q_{22}$, with the addition of isoscalar or isovector proton–neutron pairing operator in Equation (4). The $\lambda_i$ represents the Lagrange multipliers that constrain the expectation values of these operators to specified quantities of $q_i$. We solve the HFB equation repeatedly. In each time, the HFB vacuum is constrained to a different mesh point in the space of $q_i$.

After we get a set of HFB vacua with different amounts of axial quadrupole deformation, triaxial quadrupole deformation, and isoscalar (or isovector) proton–neutron pairing amplitude, the GCM state can be composed of a linear superposition of the projected HFB vacua, given by

$$|\Psi^J_{ZN\sigma}\rangle = \sum_{K,q} f^{JK}_{q\sigma} |JMK; ZN; q\rangle, \tag{8}$$

where $|JMK; ZN; q\rangle \equiv \hat{P}^J_{MK}\hat{P}^Z\hat{P}^N|\Phi(q)\rangle$. The $\hat{P}$'s are so-called projection operators which project quasiparticle vacua onto definitive angular momentum $J$ and its $z$-component $M$, proton number $Z$, and neutron number $N$ [45]. $f^{JK}_{q\sigma}$ are the weight functions, where $\sigma$ is simply a enumeration index. They can be taken as variational parameters and thus be computed by solving the Hill-Wheeler-Griffin equation [45]:

$$\sum_{K',q'} \left\{ \mathcal{H}^J_{KK'}(q;q') - E^J_\sigma \mathcal{N}^J_{KK'}(q;q') \right\} f^{JK'}_{q'\sigma} = 0, \tag{9}$$

where the Hamiltonian kernel $\mathcal{H}^J_{KK'}(q;q')$ and the norm kernel $\mathcal{N}^J_{KK'}(q;q')$ are given by:

$$\begin{aligned}\mathcal{H}^J_{KK'}(q;q') &= \langle \Phi(q)|H_{\text{eff}}\hat{P}^J_{KK'}\hat{P}^Z\hat{P}^N|\Phi(q')\rangle, \\ \mathcal{N}^J_{KK'}(q;q') &= \langle \Phi(q)|\hat{P}^J_{KK'}\hat{P}^Z\hat{P}^N|\Phi(q')\rangle.\end{aligned} \tag{10}$$

To solve the Hill-Wheeler-Griffin equation, we diagonalize the norm kernel $\mathcal{N}$ first:

$$\sum_{K',q'} \mathcal{N}^J_{KK'}(q;q') u^J_{K'k}(q') = n^J_k u^J_{Kk}(q). \tag{11}$$

The nonzero eigenvalues $n^J_k$ and corresponding eigenvectors $u^J_{Kk}(q)$ can be used to construct a set of orthonormal basis called "natural states", which are defined by

$$|k^J\rangle = \sum_{K,q} \frac{u^J_{Kk}(q)}{\sqrt{n^J_k}} |JMK; ZN; q\rangle. \tag{12}$$

The Hamiltonian can be diagonalized in the space of these natural states, and the Hill-Wheeler-Griffin equation thus can be transformed into a normal eigenvalue problem. Then we can obtain the wave functions of GCM states $|\Psi^J_{NZ\sigma}\rangle$ (see details in Refs. [46,47]). With the lowest $J = 0$ GCM states as ground states of the grandparent and grand-daughter nuclei, we can finally compute the $0\nu\beta\beta$ decay matrix element $M^{0\nu}$ in Equation (1).

## 3. Calculations and Discussion

We start by using our GCM employing an effective Hamiltonian in a valence model space. For $^{48}$Ca−Ti, we employ two sets of effective interactions to show the effect from

taking account for a larger model space. One is the KB3G interaction restricted in one-major *sd* shell [48]. The other is the SDPFMU-DB interaction in the two-major *sdpf* shell [9]. For $^{76}$Ge−Se, we set the valence space in the so-called $f5pg9$ space, which comprises the $0f_{5/2}$, $1p_{3/2}$, $1p_{1/2}$, and $0g_{9/2}$ orbits. We have employed the GCN2850 Hamiltonian that are fine tuned for relevant $0\nu\beta\beta$ decay candidate isotopes [49]. For the calculations of $^{124}$Sn−Te, $^{130}$Te−Xe, and $^{136}$Xe−Ba, we use a recently proposed shell-model effective Hamiltonian called SVD Hamiltonian [50] for the *jj*55-shell configuration space that comprises the $0g_{7/2}$, $1d_{5/2}$, $1d_{3/2}$, $2s_{1/2}$, and $0h_{11/2}$ orbitals. It has been shown that these effective interactions account successfully for the low-lying level spectra, electromagnetic and Gamow-Teller transitions, and quadrupole deformations for these nuclei, respectively [7–9,49–51]. Since the effect on $0\nu\beta\beta$ decay NME from triaxial deformation is found to be minor [32], and most of the candidate isotopes show no theoretical or experimental evidence of being triaxially deformed, we neglect the triaxial quadrupole moment $q_2 \equiv \langle Q_{22} \rangle$ in the choice of collective generator coordinates for simplicity. Instead, our GCM calculations use axial quadrupole moment $q_1 \equiv \langle Q_{20} \rangle$, as well as the proton–neutron pairing parameters $q_3 \equiv 1/2\langle P_0 + P_0^\dagger \rangle$ and $q_4 \equiv 1/2\langle S_0 + S_0^\dagger \rangle$ as generator coordinates.

We first examine the reliability of our Hamiltonian-based GCM calculation for the structural properties of the five pairs of $0\nu\beta\beta$ decay candidate nuclei of $^{48}$Ca−Ti, $^{76}$Ge−Se, $^{124}$Sn−Te, $^{130}$Te−Xe, and $^{136}$Xe−Ba, which are compared with the calculated results given by the interacting shell model (ISM) calculations based on the same effective interaction without the additional $\lambda\hat{Q}\cdot\hat{Q}$ term in Figure 1. In principal, if the Hamiltonian-based GCM and the ISM itself employ the same effective interaction in the same model space, the ISM result can therefore be taken as the "exact" solution and an adequate benchmark, because it diagonalizes the Hamiltonian exactly. A great agreement between GCM and ISM calculations for all the candidate nuclei has been shown, except for the doubly magical nucleus $^{48}$Ca in which the GCM calculation presents a slight overestimation in $B(E2; 0_1^+ \rightarrow 2_1^+)$ value. The lowest excited states in $^{48}$Ca should mainly be of particle-hole excitation, the description of which requires the incorporation of non-collective configurations.

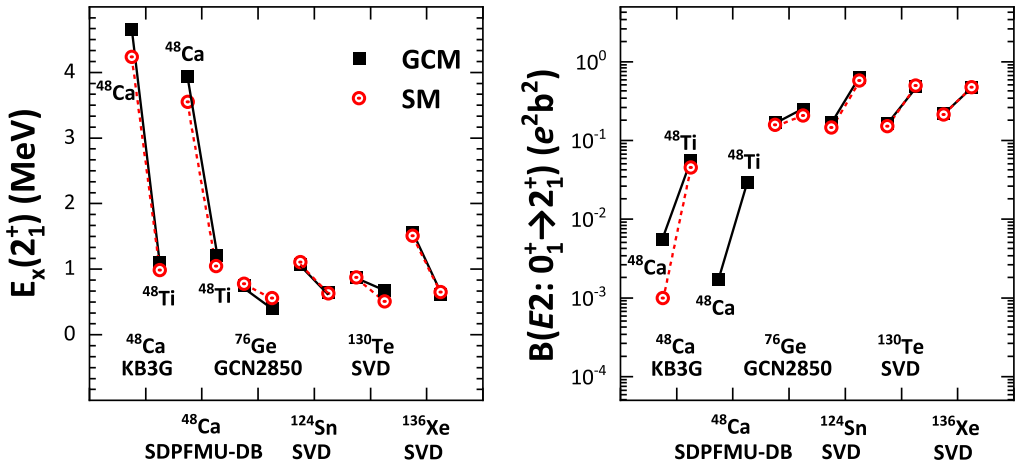


**Figure 1.** (Color online) Comparison of the calculated properties of low-lying states between our Hamiltonian-based GCM and SM for the $0\nu\beta\beta$ decay candidate nuclei of $^{48}$Ca−Ti, $^{76}$Ge−Se, $^{124}$Sn−Te, $^{130}$Te−Xe, and $^{136}$Xe−Ba, including (**left panel**) excitation energies of $2_1^+$ states $E_x(2_1^+)$ and (**right panel**) $E2$ transition strengths $B(E2; 0_1^+ \rightarrow 2_1^+)$. The SM results are taken from Refs. [7–9,49].

Before investigating the correlation of the neutrinoless double-$\beta$ decay NME with the low-lying electric quadrupole ($E2$) strength in the $0^+ \rightarrow 2^+$ transitions, we make one more test. Figure 2 shows the linear anti-correlation between the excitation energies of the first $2^+$ states and the corresponding reduced $E2$ transition probabilities $B(E2; 0^+ \rightarrow 2^+)$. As the quadrupole–quadrupole interaction becomes stronger in the effective Hamiltonian by increasing the coupling constant $\lambda$ in the extra $\lambda\hat{Q}\cdot\hat{Q}$ term, the $2^+$ energies are suppressed,

while the $B(E2;0_1^+ \rightarrow 2_1^+)$ values are significantly enhanced. Qualitatively, we see a similar evolution for $^{48}$Ti within one- and two-major-shell calculations, which employ the KB3G and SDPFMU-DB interactions, respectively. Lowered excitation energies, combining with the enhanced $B(E2)$ values, indicate that the quadrupole collectivity of low-lying states is changed smoothly along with the modification of the additional $\lambda\hat{Q}\cdot\hat{Q}$ term, as we expect.

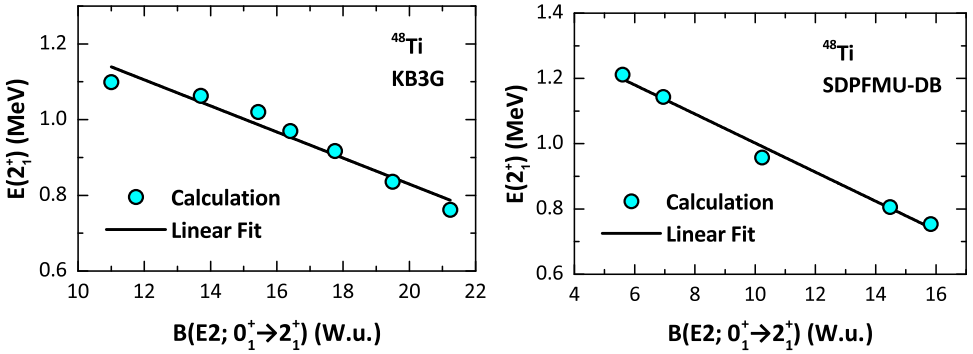


**Figure 2.** (Color online) Calculated excitation energies of the first $2^+$ state of $^{48}$Ti is linearly anti-correlated with the calculated reduced $E2$ transition probability $B(E2;0^+ \rightarrow 2^+)$. The calculations are performed in the $pf$ shell (**left panel**) and $sdpf$ shell (**right panel**), respectively.

Figure 3 plots the changes of $0\nu\beta\beta$ decay NMEs as a function of the $B(E2;0^+ \rightarrow 2^+)$ values for $^{48}$Ti. Though it is not explicitly marked in the figure, the larger constant $\lambda$ always corresponds to the larger calculated $B(E2;0^+ \rightarrow 2^+)$ values. A remarkable anti-correlation can be obtained between the $0\nu\beta\beta$ decay NMEs and the $B(E2)$ values. The same relation can be seen in both one- and two-shell calculations. The only difference is the $0\nu\beta\beta$ decay NME for $^{48}$Ca$\rightarrow$Ti decay calculated in the $sdpf$ shell is slightly larger than that in the $pf$ shell, which is in accordance with the large-scale SM calculations [9] with the omission of some cross-shell excitations. Nevertheless, the downward slope of the anti-correlation between the $0\nu\beta\beta$ decay NMEs and the $B(E2)$ values are almost the same in the the $pf$-shell and the $sdpf$-shell calculations. The result suggests that enlargement of the model space may not dramatically affect the anti-correlation between NME and quadrupole collectivity, though gradual but continual effect arising from the addition of successive shells should not be ruled out.

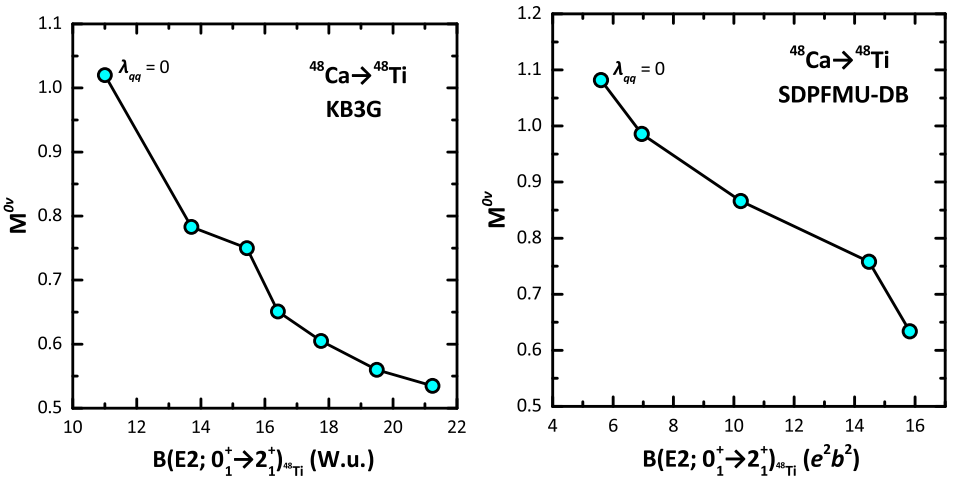


**Figure 3.** (Color online) Calculated $0\nu\beta\beta$ decay NMEs of $^{48}$Ca$-$Ti are anti-correlated with the calculated reduced $E2$ transition probabilities $B(E2;0^+ \rightarrow 2^+)$ in both $pf$-shell calculation (**left panel**) and $sdpf$-shell calculation (**right panel**).

We then turn to heavier candidate nuclei, e.g., $^{124}$Sn−Te, $^{130}$Te−Xe, and $^{136}$Xe−Ba pairs. The anti-correlations are clearly presented in these candidate pairs, as shown in Figure 4. Similarly, larger constant $\lambda$ leads to larger calculated $B(E2;0^+ \rightarrow 2^+)$ value, and results in smaller $0\nu\beta\beta$ decay NME. Since $0\nu\beta\beta$ decay occurs from the ground state of grand-parent nucleus to that of the grand-daughter nucleus, one may ask that what the correlation would be between $0\nu\beta\beta$ decay NME and the quadrupole collectivity of grand-parent nuclei. We thus plot the changes of $0\nu\beta\beta$ decay NMEs as a function of the $B(E2;0^+ \rightarrow 2^+)$ values for both the grand-parent nucleus $^{136}$Xe and the grand-daughter nucleus $^{136}$Ba in the right panel of Figure 4. Robust anti-correlations are exhibited in both $^{136}$Xe and $^{136}$Xe, though the downward slope is steeper in the grand-parent nucleus. This is due to the fact that $^{136}$Xe has 82 neutrons, which is a magical number, resulting in the characteristics of a spherical nucleus. Meanwhile, $^{136}$Ba is moderately deformed. The additional quadrupole–quadrupole interaction can barely increase the quadrupole deformation for the ground state of $^{136}$Xe owing to the robust $N = 82$ shell closure, but can remarkably enhance the quadrupole collectivity for $^{136}$Ba. A similar situation occurs in $^{48}$Ca−Ti, $^{124}$Sn−Te, and $^{130}$Te−Xe, since in all these candidate nuclei pairs, grand-parent nuclei are spherical or weakly deformed, while grand-daughter nuclei have relatively larger deformation.

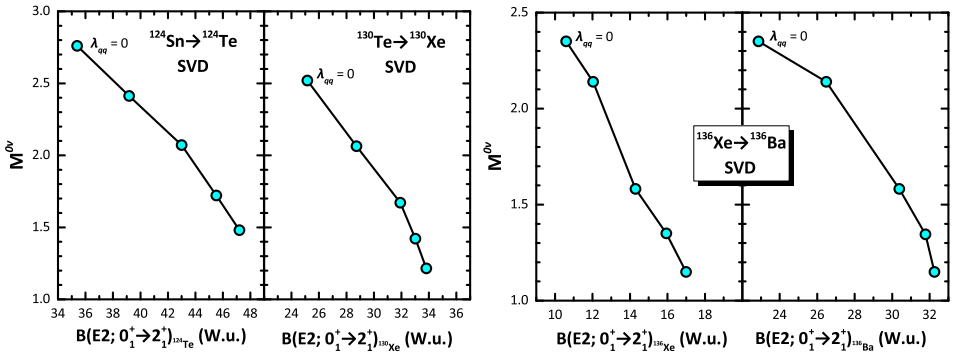


**Figure 4.** (Color online) Similar to Figure 3, but for candidate nuclei $^{124}$Sn−Te, $^{130}$Te−Xe (**left panel**) and $^{136}$Xe−Ba (**right panel**), respectively.

One may ask whether the anti-correlation between the $0\nu\beta\beta$ decay NMEs and the $E2$ transition strength merely result from the increasing difference of quadrupole collectivity between near-spherical grand-parent and deformed grand-daughter nuclei. To answer this question, we apply our analysis to $^{76}$Ge−Se candidate nuclei, since, in this pair, both grand-parent and grand-daughter nuclei are well-deformed. The results are presented in Figure 5. To illustrate the effect from enhanced quardupole-collectivity difference between grand-parent and grand-daughter nuclei, we apply two different analyses, namely, (i) the $\lambda\hat{Q}\cdot\hat{Q}$ term is added in the effective Hamiltonian used in the GCM calculations for both $^{76}$Ge and $^{76}$Se, (ii) the $\lambda\hat{Q}\cdot\hat{Q}$ term is added only for grand-daughter nucleus $^{76}$Se. Apparently, the latter case would increase the difference of quadrupole collectivity between $^{76}$Ge and $^{76}$Se. It is shown that, though the enhanced deformation difference between $^{76}$Ge and $^{76}$Se leads to a steeper downward slope of the $0\nu\beta\beta$ decay NME against the reduced $E2$ transition probability in the latter analysis, the anti-correlation between them still exists in the first analysis, in which the quadrupole collectivity is enhanced almost equally in $^{76}$Ge and $^{76}$Se.

To show the thorough interrelation between the $0\nu\beta\beta$ decay NMEs and the $E2$ strengths, Figure 6 summarizes our calculated results. As noted, the anti-correlation of $0\nu\beta\beta$ decay NMEs with the $E2$ strengths exists for investigated candidate nuclei in a universal way. The downward slopes are similar in both the $pf$-shell and $sdpf$-shell case of $^{48}$Ca−Ti, as well as in the case of $^{48}$Ca−Ti. The anti-correlated trend is even more drastic in the heavier candidates $^{124}$Sn−Te, $^{130}$Te−Xe, and $^{136}$Xe−Ba. We also plot the adopted values of $B(E2;0^+ \rightarrow 2^+)$ from experiments [52], shown as vertical shades. The width of the shade displays the uncertainty of measured reduced $E2$ transition probability. It can be seen

that the calculated $B(E2;0^+ \rightarrow 2^+)$ value without the artificial quadrupole–quadrupole interaction, which is denoted by the starting point of each curve, shows non-negligible discrepancy when compared with adopted values. It should be noted that, the more accurate correlation between $0\nu\beta\beta$ decay NME and $E2$ strength can be determined if we can obtain a better description of reduced $E2$ transition probability, and hence potentially help us to reduce the uncertainty of the $0\nu\beta\beta$ decay NME.

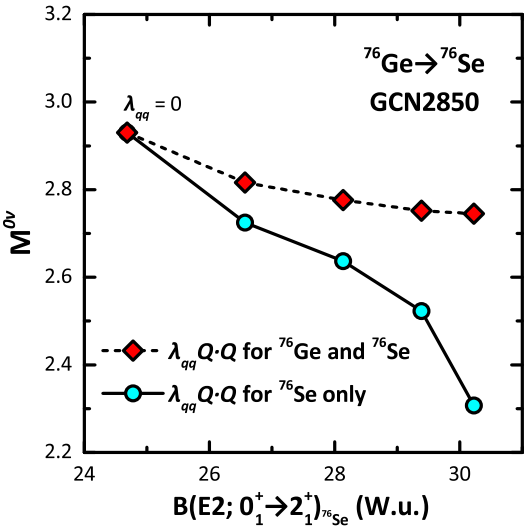


**Figure 5.** (Color online) Calculated $0\nu\beta\beta$ decay NMEs of $^{76}$Ge−Se changing against the calculated reduced $E2$ transition probabilities $B(E2;0^+ \rightarrow 2^+)$. The calculation adding $\lambda\hat{Q}\cdot\hat{Q}$ term for both $^{76}$Ge and $^{76}$Se is denoted by red diamonds and a dash line, while the calculation adding $\lambda\hat{Q}\cdot\hat{Q}$ term for only $^{76}$Se is shown as cyan circles and a solid line.

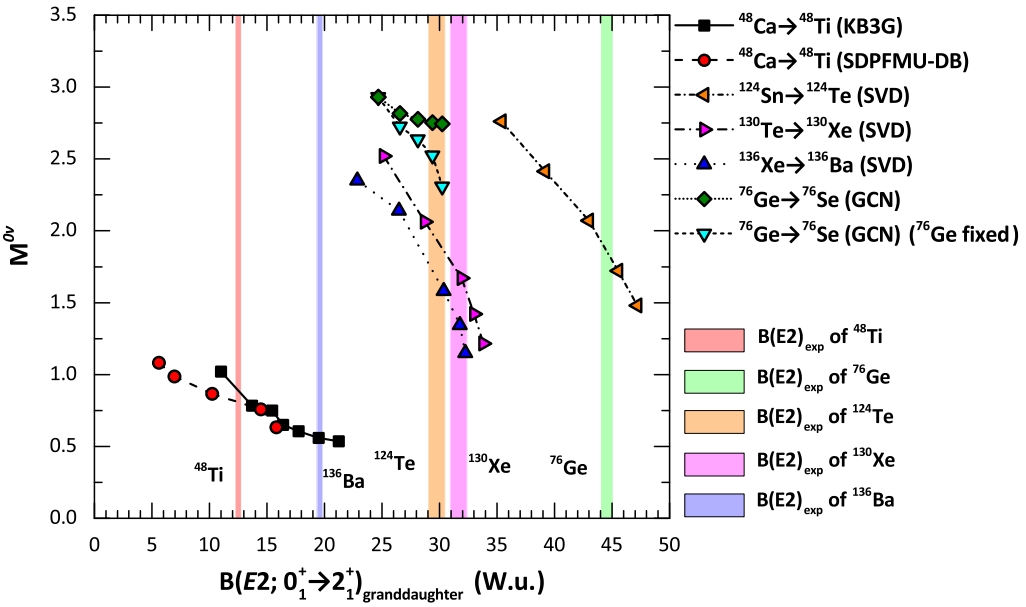


**Figure 6.** (Color online) Calculated $0\nu\beta\beta$ decay NMEs of all investigated candidate nuclei changing against the calculated reduced $E2$ transition probabilities $B(E2;0^+ \rightarrow 2^+)$. The vertical shades represent the adopted values of $B(E2;0^+ \rightarrow 2^+)$.

## 4. Conclusions

In this paper, we apply a detailed analysis of the interrelation between $0\nu\beta\beta$ decay NMEs and $E2$ transition rates $B(E2;0^+ \rightarrow 2^+)$, using the Hamiltonian-based GCM built on the configuration mixing of symmetry-restored intrinsic basis states. The calculated

$0\nu\beta\beta$ decay NMEs are clearly anti-correlated with the calculated transition rates of the collective quadrupole excitation from the ground state to the first $2^+$ state in response to artificial changes of quadrupole–quadrupole contributions in effective Hamiltonians. The anti-correlation is more remarkable in the decay from a spherical or weakly deformed grandparent nucleus than a more deformed grand-daughter nucleus. Therefore, we conclude that a reliable description of the reduced collective $E2$ transition probability would be useful for reducing the uncertainties of the $0\nu\beta\beta$ decay NME.

Another interesting study would be the correlation of $0\nu\beta\beta$ decay NME with $E2$ strength for $^{150}$Nd$-$Sm decay process. It is because $^{150}$Nd$-$Sm is the only candidate nuclei pair of which the grandparent $^{150}$Nd has larger quadrupole deformation compared with the grand-daughter $^{150}$Sm. However, to compute the NME of the heaviest candidate $^{150}$Nd$-$Sm with Hamiltonian-based GCM, the first issue that must be grappled with is what to use for the effective Hamiltonian. Since $^{150}$Nd consists of 60 protons and 90 neutrons, the calculation should be carried out in the valence space between the proton and neutron 50 to 126 shell closures. The effective Hamiltonian for this extremely large model space is beyond the current capability. To overcome this difficulty, an implementation of multiple-shell valence-space Hamiltonians derived from non-perturbative *ab initio* methods, such as in-medium similarity renormalization group (IM-SRG) [53] or CC [54] method, would be of great importance. Recently, the valence-space Hamiltonians derived from both IM-SRG [55,56] and CC method [57] has been used to explore the open-shell nuclei in one single shell. The extension of the *ab initio* valence-space Hamiltonian to multiple shells is still in progress.

Finally, it should be mentioned that we only discuss the NME of $0\nu\beta\beta$ decay from the ground-state of grandparent nucleus to the ground-state of grand-daughter nucleus here. Actually, the decay to the low-lying excited states of the grand-daughter nucleus should also be taken into account if it is allowed energetically. The NME of this process is expected to be strongly suppressed by the phase-space factor in the standard light left-handed Majorana neutrino exchange mechanism [58,59]. Nevertheless, it may considerably contribute to the NME in the non-standard mechanism. Further investigation of $0\nu\beta\beta$ decay NME to the lowest $2_1^+$ state of grand-daughter nucleus within the framework of Hamiltonian-based GCM would be a desirable next step in future work.

**Author Contributions:** Conceptualization, C.J., C.Y. and J.Y.; methodology, C.J.; numerical calculations and analyses, C.J.; writing—original draft preparation, C.J.; writing—review and editing, C.Y. and J.Y. All authors have read and agreed to the published version of the manuscript.

**Funding:** This research was funded by the National Natural Science Foundation of China (Grant Nos. 12275369 and 12141501) and the Fundamental Research Funds for the Central Universities, Sun Yat-sen University (Grant No. 22qntd3101). C. X. Yuan acknowledges the support from the Guangdong Major Project of Basic and Applied Basic Research 2021B0301030006.

**Institutional Review Board Statement:** Not applicable.

**Informed Consent Statement:** Not applicable.

**Data Availability Statement:** Data are contained within the article.

**Acknowledgments:** We thank C. W. Johnson for fruitful discussions.

**Conflicts of Interest:** The authors declare no conflict of interest.

## Abbreviations

The following abbreviations are used in this manuscript:

| | |
|---|---|
| $0\nu\beta\beta$ | Neutrinoless double-$\beta$ decay |
| NME | Nuclear matrix element |
| $E2$ | Electric quadrupole |
| ISM | Interacting shell model |
| IBM | Interacting boson method |
| QRPA | Quasiparticle random phase approximation |
| GCM | Generator-coordinate method |
| EDF | Energy density functional |
| IM-GCM | In-medium generator-coordinate method |
| CC | Coupled-cluster method |
| HFB | Hartree-Fock-Bogliubov |
| IM-SRG | In-medium similarity renormalization group |
| GT | Gamow-Teller |
| SRC | Short range correlation |

## References


1. Avignone, F.T.; Elliott, S.R.; Engel, J. Double beta decay, Majorana neutrinos, and neutrino mass. *Rev. Mod. Phys.* **2008**, *80*, 481–516. [CrossRef]
2. Caurier, E.; Menéndez, J.; Nowacki, F.; Poves, A. Influence of Pairing on the Nuclear Matrix Elements of the Neutrinoless $\beta\beta$ Decays. *Phys. Rev. Lett.* **2008**, *100*, 052503. [CrossRef]
3. Menéndez, J.; Poves, A.; Caurier, E.; Nowacki, F. Disassembling the nuclear matrix elements of the neutrinoless $\beta\beta$ decay. *Nucl. Phys. A* **2009**, *818*, 139–151. . [CrossRef]
4. Horoi, M.; Stoica, S. Shell model analysis of the neutrinoless double-$\beta$ decay of $^{48}$Ca. *Phys. Rev. C* **2010**, *81*, 024321. [CrossRef]
5. Horoi, M. Shell model analysis of competing contributions to the double-$\beta$ decay of $^{48}$Ca. *Phys. Rev. C* **2013**, *87*, 014320. [CrossRef]
6. Horoi, M.; Brown, B.A. Shell-Model Analysis of the $^{136}$Xe Double Beta Decay Nuclear Matrix Elements. *Phys. Rev. Lett.* **2013**, *110*, 222502. [CrossRef]
7. Neacsu, A.; Horoi, M. Shell model studies of the $^{130}$Te neutrinoless double-$\beta$ decay. *Phys. Rev. C* **2015**, *91*, 024309. [CrossRef]
8. Horoi, M.; Neacsu, A. Shell model predictions for $^{124}$Sn double-$\beta$ decay. *Phys. Rev. C* **2016**, *93*, 024308. [CrossRef]
9. Iwata, Y.; Shimizu, N.; Otsuka, T.; Utsuno, Y.; Menéndez, J.; Honma, M.; Abe, T. Large-Scale Shell-Model Analysis of the Neutrinoless $\beta\beta$ Decay of $^{48}$Ca. *Phys. Rev. Lett.* **2016**, *116*, 112502. [CrossRef]
10. Sen'kov, R.A.; Horoi, M. Shell-model calculation of neutrinoless double-$\beta$ decay of $^{76}$Ge. *Phys. Rev. C* **2016**, *93*, 044334. [CrossRef]
11. Barea, J.; Kotila, J.; Iachello, F. Limits on Neutrino Masses from Neutrinoless Double-$\beta$ Decay. *Phys. Rev. Lett.* **2012**, *109*, 042501. [CrossRef]
12. Barea, J.; Kotila, J.; Iachello, F. Nuclear matrix elements for double-$\beta$ decay. *Phys. Rev. C* **2013**, *87*, 014315. [CrossRef]
13. Barea, J.; Kotila, J.; Iachello, F. $0\nu\beta\beta$ and $2\nu\beta\beta$ nuclear matrix elements in the interacting boson model with isospin restoration. *Phys. Rev. C* **2015**, *91*, 034304. [CrossRef]
14. Šimkovic, F.; Pantis, G.; Vergados, J.D.; Faessler, A. Additional nucleon current contributions to neutrinoless double $\beta$ decay. *Phys. Rev. C* **1999**, *60*, 055502. [CrossRef]
15. Rodin, V.A.; Faessler, A.; Šimkovic, F.; Vogel, P. Uncertainty in the $0\nu\beta\beta$ decay nuclear matrix elements. *Phys. Rev. C* **2003**, *68*, 044302. [CrossRef]
16. Kortelainen, M.; Civitarese, O.; Suhonen, J.; Toivanen, J. Short-range correlations and neutrinoless double beta decay. *Phys. Lett. B* **2007**, *647*, 128–132. . [CrossRef]
17. Kortelainen, M.; Suhonen, J. Improved short-range correlations and $0\nu\beta\beta$ nuclear matrix elements of $^{76}$Ge and $^{82}$Se. *Phys. Rev. C* **2007**, *75*, 051303(R). [CrossRef]
18. Šimkovic, F.; Faessler, A.; Rodin, V.; Vogel, P.; Engel, J. Anatomy of the $0\nu\beta\beta$ nuclear matrix elements. *Phys. Rev. C* **2008**, *77*, 045503. [CrossRef]
19. Šimkovic, F.; Faessler, A.; Müther, H.; Rodin, V.; Stauf, M. $0\nu\beta\beta$-decay nuclear matrix elements with self-consistent short-range correlations. *Phys. Rev. C* **2009**, *79*, 055501. [CrossRef]
20. Šimkovic, F.; Faessler, A.; Vogel, P. $0\nu\beta\beta$ nuclear matrix elements and the occupancy of individual orbits. *Phys. Rev. C* **2009**, *79*, 015502. [CrossRef]
21. Mustonen, M.T.; Engel, J. Large-scale calculations of the double-$\beta$ decay of $^{76}$**Ge**, $^{130}$**Te**, $^{136}$**Xe**, and $^{150}$**Nd** in the deformed self-consistent Skyrme quasiparticle random-phase approximation. *Phys. Rev. C* **2013**, *87*, 064302. [CrossRef]
22. Šimkovic, F.; Rodin, V.; Faessler, A.; Vogel, P. $0\nu\beta\beta$ and $2\nu\beta\beta$ nuclear matrix elements, quasiparticle random-phase approximation, and isospin symmetry restoration. *Phys. Rev. C* **2013**, *87*, 045501. [CrossRef]
23. Faessler, A.; González, M.; Kovalenko, S.; Šimkovic, F. Arbitrary mass Majorana neutrinos in neutrinoless double beta decay. *Phys. Rev. D* **2014**, *90*, 096010. [CrossRef]

24. Hyvärinen, J.; Suhonen, J. Nuclear matrix elements for $0\nu\beta\beta$ decays with light or heavy Majorana-neutrino exchange. *Phys. Rev. C* **2015**, *91*, 024613. [CrossRef]
25. Fang, D.L.; Faessler, A.; Šimkovic, F. $0\nu\beta\beta$-decay nuclear matrix element for light and heavy neutrino mass mechanisms from deformed quasiparticle random-phase approximation calculations for $^{76}$Ge,$^{82}$ Se,$^{130}$ Te,$^{136}$ Xe, and $^{150}$Nd with isospin restoration. *Phys. Rev. C* **2018**, *97*, 045503. [CrossRef]
26. Rodríguez, T.R.; Martínez-Pinedo, G. Energy Density Functional Study of Nuclear Matrix Elements for Neutrinoless $\beta\beta$ Decay. *Phys. Rev. Lett.* **2010**, *105*, 252503. [CrossRef]
27. Vaquero, N.L.; Rodríguez, T.R.; Egido, J.L. Shape and Pairing Fluctuation Effects on Neutrinoless Double Beta Decay Nuclear Matrix Elements. *Phys. Rev. Lett.* **2013**, *111*, 142501. [CrossRef]
28. Rodríguez, T.R.; Martínez-Pinedo, G. Neutrinoless $\beta\beta$ decay nuclear matrix elements in an isotopic chain. *Phys. Lett. B* **2013**, *719*, 174–178. [CrossRef]
29. Yao, J.M.; Song, L.S.; Hagino, K.; Ring, P.; Meng, J. Systematic study of nuclear matrix elements in neutrinoless double-$\beta$ decay with a beyond-mean-field covariant density functional theory. *Phys. Rev. C* **2015**, *91*, 024316. [CrossRef]
30. Yao, J.M.; Engel, J. Octupole correlations in low-lying states of $^{150}$Nd and $^{150}$Sm and their impact on neutrinoless double-$\beta$ decay. *Phys. Rev. C* **2016**, *94*, 014306. [CrossRef]
31. Hinohara, N.; Engel, J. Proton-neutron pairing amplitude as a generator coordinate for double-$\beta$ decay. *Phys. Rev. C* **2014**, *90*, 031301. [CrossRef]
32. Jiao, C.F.; Engel, J.; Holt, J.D. Neutrinoless double-$\beta$ decay matrix elements in large shell-model spaces with the generator-coordinate method. *Phys. Rev. C* **2017**, *96*, 054310. [CrossRef]
33. Jiao, C.F.; Horoi, M.; Neacsu, A. Neutrinoless double-$\beta$ decay of $^{124}$Sn, $^{130}$Te, and $^{136}$Xe in the Hamiltonian-based generator-coordinate method. *Phys. Rev. C* **2018**, *98*, 064324. [CrossRef]
34. Jiao, C.F.; Johnson, C.W. Union of rotational and vibrational modes in generator-coordinate-type calculations, with application to neutrinoless double-$\beta$ decay. *Phys. Rev. C* **2019**, *100*, 031303. [CrossRef]
35. Yao, J.M.; Bally, B.; Engel, J.; Wirth, R.; Rodríguez, T.R.; Hergert, H. Ab Initio Treatment of Collective Correlations and the Neutrinoless Double Beta Decay of $^{48}$Ca. *Phys. Rev. Lett.* **2020**, *124*, 232501. [CrossRef]
36. Novario, S.; Gysbers, P.; Engel, J.; Hagen, G.; Jansen, G.R.; Morris, T.D.; Navrátil, P.; Papenbrock, T.; Quaglioni, S. Coupled-Cluster Calculations of Neutrinoless Double-$\beta$ Decay in $^{48}$Ca. *Phys. Rev. Lett.* **2021**, *126*, 182502. [CrossRef]
37. Engel, J.; Menéndez, J. Status and future of nuclear matrix elements for neutrinoless double-beta decay: A review. *Rep. Prog. Phys.* **2017**, *80*, 046301. [CrossRef] [PubMed]
38. Vogel, P. Nuclear structure and double beta decay. *J. Phys. G Nucl. Part. Phys.* **2012**, *39*, 124002. [CrossRef]
39. Yao, J.; Meng, J.; Niu, Y.; Ring, P. Beyond-mean-field approaches for nuclear neutrinoless double beta decay in the standard mechanism. *Prog. Part. Nucl. Phys.* **2022**, *126*, 103965. [CrossRef]
40. Caurier, E.; Nowacki, F.; Poves, A. Nuclear-structure aspects of the neutrinoless $\beta\beta$-decays. *Eur. Phys. J. A* **2008**, *36*, 195–200. [CrossRef]
41. Fang, D.L.; Faessler, A.; Rodin, V.; Šimkovic, F. Neutrinoless double-$\beta$ decay of deformed nuclei within quasiparticle random-phase approximation with a realistic interaction. *Phys. Rev. C* **2011**, *83*, 034320. [CrossRef]
42. Zelevinsky, V.; Auerbach, N.; Loc, B.M. Nuclear structure features of Gamow-Teller excitations. *Phys. Rev. C* **2017**, *96*, 044319. [CrossRef]
43. Horoi, M.; Neacsu, A.; Stoica, S. Statistical analysis for the neutrinoless double-$\beta$-decay matrix element of $^{48}$Ca. *Phys. Rev. C* **2022**, *106*, 054302. [CrossRef]
44. Goodman, A.L. Advances in Nuclear Physics. In *Advances in Nuclear Physics*; Negele, J.V., Vogt, E., Eds.; Plenum Press: New York, NY, USA, 1979; Volume 11, p. 263.
45. Ring, P.; Schuck, P. *The Nuclear Many-Body Problem*; Springer: Berlin, Germany, 1980.
46. Rodríguez, T.R.; Egido, J.L. Triaxial angular momentum projection and configuration mixing calculations with the Gogny force. *Phys. Rev. C* **2010**, *81*, 064323. [CrossRef]
47. Yao, J.M.; Meng, J.; Ring, P.; Vretenar, D. Configuration mixing of angular-momentum-projected triaxial relativistic mean-field wave functions. *Phys. Rev. C* **2010**, *81*, 044311. [CrossRef]
48. Poves, A.; Sánchez-Solano, J.; Caurier, E.; Nowacki, F. Shell model study of the isobaric chains A = 50, A = 51 and A = 52. *Nucl. Phys. A* **2001**, *694*, 157–198. . [CrossRef]
49. Gniady, A.; Caurier, E.; Nowacki, F. *(unpublised)*.
50. Qi, C.; Xu, Z.X. Monopole-optimized effective interaction for tin isotopes. *Phys. Rev. C* **2012**, *86*, 044323. [CrossRef]
51. Caurier, E.; Martínez-Pinedo, G.; Nowacki, F.; Poves, A.; Zuker, A.P. The shell model as a unified view of nuclear structure. *Rev. Mod. Phys.* **2005**, *77*, 427–488. [CrossRef]
52. Pritychenko, B.; Birch, M.; Singh, B.; Horoi, M. Tables of E2 transition probabilities from the first 2+ states in even–even nuclei. *At. Data Nucl. Data Tables* **2016**, *107*, 1–139. [CrossRef]
53. Bogner, S.K.; Hergert, H.; Holt, J.D.; Schwenk, A.; Binder, S.; Calci, A.; Langhammer, J.; Roth, R. Nonperturbative Shell-Model Interactions from the In-Medium Similarity Renormalization Group. *Phys. Rev. Lett.* **2014**, *113*, 142501. [CrossRef]
54. Hagen, G.; Papenbrock, T.; Hjorth-Jensen, M.; Dean, D.J. Coupled-cluster computations of atomic nuclei. *Rep. Prog. Phys.* **2014**, *77*, 096302. [CrossRef]

55. Stroberg, S.R.; Hergert, H.; Holt, J.D.; Bogner, S.K.; Schwenk, A. Ground and excited states of doubly open-shell nuclei from ab initio valence-space Hamiltonians. *Phys. Rev. C* **2016**, *93*, 051301. [CrossRef]
56. Stroberg, S.R.; Calci, A.; Hergert, H.; Holt, J.D.; Bogner, S.K.; Roth, R.; Schwenk, A. Nucleus-Dependent Valence-Space Approach to Nuclear Structure. *Phys. Rev. Lett.* **2017**, *118*, 032502. [CrossRef]
57. Jansen, G.R.; Schuster, M.D.; Signoracci, A.; Hagen, G.; Navrátil, P. Open *sd*-shell nuclei from first principles. *Phys. Rev. C* **2016**, *94*, 011301. [CrossRef]
58. Tomoda, T. $0^+ \to 2^+$ neutrinoless $\beta\beta$ decay of $^{76}$Ge. *Nucl. Phys. A* **1988**, *484*, 635–646. [CrossRef]
59. Fang, D.L.; Faessler, A. Nuclear matrix elements for the $0\nu\beta\beta(0^+ \to 2^+)$ decay of $^{76}$Ge within the two-nucleon mechanism. *Phys. Rev. C* **2021**, *103*, 045501. [CrossRef]